7-2015

Atom Probe Study of Irradiation-Enhanced α' Precipitation in Neutron-Irradiated Fe–Cr Model Alloys

Yaqiao Wu
Boise State University

Atom Probe Study of Irradiation-Enhanced α′ Precipitation in Neutron-Irradiated Fe-Cr Model Alloys

Wei-Ying Chen
Department of Nuclear, Plasma and Radiological Engineering
University of Illinois
Urbana, IL

Yinbin Miao
Department of Nuclear, Plasma and Radiological Engineering
University of Illinois
Urbana, IL

Yaqiao Wu
Department of Materials Science and Engineering
Boise State University
Boise, ID

and

Center for Advanced Energy Studies
Idaho Falls, ID

Carolyn A. Tomchik
Department of Nuclear, Plasma and Radiological Engineering
University of Illinois
Urbana, IL

Kun Mo
Department of Nuclear, Plasma and Radiological Engineering
University of Illinois
Urbana, IL

Jian Gan
Idaho National Laboratory
Idaho Falls, ID

Maria A. Okuniewski
Idaho National Laboratory
Idaho Falls, ID

Stuart A. Maloy
Los Alamos National Laboratory
Los Alamos, NM

James F. Stubbins
Department of Nuclear, Plasma and Radiological Engineering
University of Illinois
Urbana, IL

1. Introduction

Ferritic-martensitic (F/M) steels are considered as lead candidate materials for Gen IV fission reactors and fusion reactors due to their superior swelling resistance, higher thermal conductivity, lower thermal expansion and adequate mechanical properties [1][2]. However, F/M steels exhibit low-temperature irradiation-induced embrittlement, which poses problems for their use below 400°C [3]. In addition to the irradiation temperature limitations, Cr contents (2-18%) have been shown to substantially affect the irradiation-induced embrittlement and hardening [4][5]. The formation of dislocation loops and the Cr-rich α′ precipitates under certain irradiation conditions is partly responsible for the embrittlement process.

Fe-Cr model alloys have been used to study the irradiation effects in F/M steels for decades. Earlier transmission electron microscopy (TEM) investigations on bcc Fe-Cr model alloys irradiated with heavy-ions and neutrons have considerably extended the understanding of the effects of Cr concentration and irradiation temperatures on the formation of the irradiation-induced dislocation loops [5][6][7][8][9][10].

α′ precipitates are Cr-rich bcc phase coherent to the Fe-rich α matrix. TEM is not optimal for the study of α′ precipitates because of the small misfit in lattice parameter between Fe-rich α and Cr-rich α′ phases and the small difference in atomic mass between Fe and Cr atoms [11]. Instead, atom probe tomography (APT) has been shown to be the best tool for the characterization of these precipitates. Earlier APT studies focused on the aging effects in Fe-Cr alloys with higher Cr concentrations (>20%) [11][12][13][14][15]. However, the Cr concentration of engineering importance for nuclear structure materials is 9-12%, and the APT studies for this range have been lacking [16][17].

In order to evaluate the performance of F/M steels, a systematic understanding of the irradiation effects as a function of Cr concentration, irradiation temperatures and irradiation doses is important. In this work, poly-crystalline and single-crystal model alloys were irradiated with neutrons at 300 and 450°C to doses of 0.01, 0.1 and 1 dpa. The irradiated and unirradiated specimens were investigated with APT to study the irradiation-enhanced α′ precipitation.

2. Materials and Experimental Procedure

The materials examined in this study were poly-crystalline and single-crystalline Fe-Cr model alloys with nominal Cr concentration of 10 at.%, and 14 at.% Cr, respectively. The poly-crystalline specimens have an average grain size of 180 μm. The chemical composition was measured by Carpenter Technology Corporation as 0.023 C, 0.006 N, <0.021 Al, <0.02 Si, <0.009 P, 0.004 S, 9.65 Cr, <0.01 Mn, 0.019 Co, 0.009 Ni, <0.009 Cu, <0.006 Mo (at.%). The single-crystal specimens were made in Los Alamos National Laboratory by Czochralski growth process. During the growth process, Cr was lost through evaporation, resulting in a crystal with decreasing Cr concentration along its length. The specimens were taken from cross-sectional slices of the original bar material and, therefore, had different Cr concentrations. The Cr concentration was, however, homogeneous inside individual specimens. The impurity level of single-crystalline specimens was similar to poly-crystalline specimens. The composition of single crystalline specimens was measured with APT. Table 1 summarizes the Cr contents x_{Cr} and the corresponding irradiation conditions of all specimens where the error was the statistical uncertainty estimated by the peak decomposition routine of IVAS^{TM} software. To avoid confusion, single crystal specimens and poly-crystalline specimens were labeled with a SC and a PC after them, respectively.

The specimens were irradiated in the Advanced Test Reactor at Idaho National Laboratory (INL). Three irradiation doses of 0.01, 0.1 and 1 dpa, and two irradiation temperatures of 300 and 450°C were examined. The archive materials were also characterized. After irradiation, the specimens were mechanically polished and then electro-polished to achieve mirror-like surface condition in the Materials and Fuels Complex at INL. The sample preparation and APT analysis were performed in the Center for Advanced Energy Studies using focused ion beam, and a CAMECA local electrode atom probe of model 4000X HR with voltage pulsing mode at 50 kelvin of 20% pulse fraction. Multiple APT tips were analyzed for each irradiation condition to verify data reliability and consistency.

3. Data Analysis

The 3D grid of concentration was generated with IVAS software with a delocalization value of 3.0 nm (x, y) and 1.5 nm (z), and a voxel size of 1 nm. Three analysis techniques were performed: isoconcentration surface, frequency distribution analysis and proximity histogram [18][19][20][21].

The Cr-rich α′ precipitates were visualized with the use of isoconcentration surfaces, or isosurfaces for short. An isosurface is a surface of designated concentration in three dimensions. In order to make comparison among specimens of various characteristics (Cr content, irradiation temperature, dose etc.), one single Cr concentration was used to define the α′ precipitates. In this study, 20%Cr was selected since it reveals suitably the precipitates in all of the 1 dpa specimens.

The size, density and volume fraction of α′ precipitates were obtained by measuring the precipitates defined by the isosurfaces of 20%Cr. The density N_p was calculated according to Eq-1 and Eq-2 [22].

$$N_p = \frac{N_{\alpha1} + 0.5 \times N_{\alpha2}}{V} \qquad (Eq-1)$$

$$V = \frac{N_{Fe,Cr}/(detection\ efficiency)}{a^3/2} \qquad (Eq-2)$$

Where $N_{\alpha1}$ is the number of α' precipitates well inside the boundary of the reconstruction data. $N_{\alpha2}$ is the number of α' precipitates located at the edge of the boundary. As an estimate, half of the precipitates at the edge of the boundary were assumed to contribute to the density. V is the specimen volume estimated using lattice constant a (2.87 Å [23]), total number of Fe and Cr ions, $N_{Fe,Cr}$, and the detection efficiency.

For the precipitates well inside the boundary of the reconstruction data, the sizes were clearly defined by the isosurfaces and could be readily obtained. For precipitates located at the edge of the boundary, however, their sizes were not obtainable. Therefore, the mean size of α' precipitates was calculated by considering only the precipitates well inside the boundary. The volume fraction of α' precipitates was obtained through dividing the total volume inside isosurfaces by the specimen volume *V*.

The frequency distribution analysis reveals the degree of Cr segregation in a statistical fashion. The descriptions of frequency distribution analysis in APT can be found in [19]. In this study, the Pearson coefficient, μ, was used to quantify the deviation of the measured frequency distribution *e(n)* from the binomial distribution *f(n)*,

$$\mu = \sqrt{\frac{\chi^2}{N + \chi^2}} \qquad (Eq-3)$$

The χ^2 was defined as

$$\chi^2 = \sum_{n=0}^{n_b} \frac{(e(n) - f(n))^2}{f(n)} \qquad (Eq-4)$$

where n_b is the block size. The Pearson coefficient μ ranges between 0 and 1, corresponding to random distribution and complete decomposition, respectively. Smaller block size is more effective for detecting small-scale composition variations. However, when the block size is too small, spatial information is lost as nearby atoms are assigned into different blocks during the sampling process **[19][24]**. Based on recent APT studies on similar materials [25][26], a block size of 100 atoms was selected in this work.

A proximity histogram, or proxigram, was used to study the Cr concentration profile along the phase boundary normal of α' precipitates. A comprehensive introduction of proxigram was given in [21]. Multiple precipitates of similar sizes were combined to plot the proxigram in this study for better statistical significance. Alternatively, the Cr concentration profile of a single α' precipitate could be acquired by the use of the region of interest (ROI) across the precipitate boundary. However, the boundary curvatures of the α' precipitates in this study were too large (due to the small sizes of 1-2 nm) for ROI method to appropriately accommodate [18].

4. Results

4.1. Isoconcentration Surface Analysis

For the specimens of a dose equal and less than 0.1 dpa, few α' precipitates were found by using isosurfaces of 20%Cr or lower. Contrarily, α' precipitates were observed in all of the 1 dpa specimens. Figure 1 shows the 20%Cr isosurface and **Figure 2** shows the size distribution within the 1 dpa specimens. Table 2 summarized the size $\overline{r_{\alpha'}}$, density $N_{\alpha'}$ and volume fraction $f_{\alpha'}$ of α' precipitates.

The morphologies of α' precipitates in 1 dpa specimens varied with x_{Cr} and T_{irr}. The size was larger in 300°C than in 450°C irradiated samples. On the other hand, size increases with x_{Cr}, but less significantly. Therefore, it is suggested that $\overline{r_{\alpha'}}$ was controlled more by the T_{irr} than by x_{Cr} within the temperature and composition range of this study.

Both the T_{irr} and x_{Cr} substantially affected the $N_{\alpha'}$. Specimens with higher x_{Cr} and lower T_{irr} exhibited higher $N_{\alpha'}$. Since $\overline{r_{\alpha'}}$ were close to 1 nm for all conditions, the volume $f_{\alpha'}$ is essentially determined by $N_{\alpha'}$. The 300°C Fe16Cr-SC has the highest $f_{\alpha'}$, followed sequentially by 450°C Fe13Cr-SC, 300°C Fe10Cr-PC and 450°C Fe10Cr-PC, which is qualitatively in accordance with the phase diagram prediction [27][28].

4.2. Proximity Histogram Analysis

The proxigram analysis was performed on 1 dpa specimens. The α′ precipitates were divided into several size groups, and a proxigram for each group was generated. Figure 3 is the proxigram of the selected size groups in 1 dpa Fe10Cr-PC specimen irradiated at 300 °C. The Cr concentration profiles of different size groups were coincident. The Cr concentration increased continuously toward the core of precipitates without forming a plateau.

The Cr concentrations at the core of precipitates increased with precipitate sizes as shown in Figure 3. In more detail, Figure 4 shows the core Cr concentration as a function of precipitate size in 1 dpa Fe10Cr-PC specimens irradiated at 300 and 450°C. No significant difference was observed between the two temperatures. The core Cr concentration (~55%) of precipitates with a size around 1.1 nm was coherent with earlier APT investigations on 0.6 dpa Fe9Cr [29], implying that the effect of irradiation doses from 0.6 dpa to 1 dpa on the core Cr concentration was insignificant. The implication of the core Cr concentration dependence on the precipitate size is discussed in the discussion session.

4.3. Frequency Distribution Analysis

For specimens with an irradiation dose lower than 1 dpa, it is difficult to use isosurface to reveal α′ precipitates. Instead, frequency distribution analysis was found useful to study the early stage of Cr segregations. The frequency distribution and the corresponding binomial distribution of Fe-Cr specimens are shown in Figure 5, Figure 6 and Figure 7. The μ-index derived from the frequency distribution is shown in Figure 8. As Figure 5 shows, the frequency distributions of the un-irradiated specimens are very close to the binomial distributions, indicating negligible α′ phase in the as-received specimens.

Up to 0.1 dpa, the frequency distributions of irradiated Fe10Cr-PC specimens are similar to as-received specimen. No evident segregation of Cr atoms was detected. At 1 dpa, however, considerable deviation, with frequencies moved toward two sides, was observed as shown in Figure 6. In addition, the deviation between the observed distribution and the binomial distribution was higher in 300°C than in 450°C irradiated samples.

For irradiated Fe-Cr single crystals (higher x_{Cr}), Cr segregation increased with irradiation dose. Some Cr segregations at lower doses of 0.01 and 0.1 dpa were detected, which was different from Fe10Cr-PC specimens. This result indicated that the Cr segregations began earlier in Fe-Cr alloys with higher x_{Cr}. Because of the variations in x_{Cr}, it was more difficult to evaluate the T_{irr} effects on the Cr segregations in single-crystalline specimens. For instance, the 0.1 dpa Fe10Cr-SC specimen irradiated at 300°C exhibited a particularly low Cr content (10.02%), which resulted in lower degree of Cr segregation.

5. Discussion

5.1. Effects of irradiation dose on the α′ precipitation

Precipitation kinetics of the α′ phase is much faster under irradiation than under thermal aging conditions alone due to irradiation-enhanced diffusivity [15][30]. Figure 9 shows a compilation of experimental data showing the evolution of $f_{α'}$ for Fe-Cr alloys with Cr contents x_{Cr} = 9-10% irradiated at T_{irr} = 300-325°C. The dashed line is the $f_{α'}$ for Fe-Cr with x_{Cr} = 9.65% at 300°C predicted by the phase diagram using lever rule [28]. Except for one data point from [30], $f_{α'}$ remains below the saturation limit as it evolves with irradiation. Provided the sensitivity of 20%Cr isosurface, a threshold dose between 0.1 to 0.6 dpa was suggested for detecting the formation of α′ precipitates in Fe10Cr irradiated at ~300°C.

Beyond 0.6 dpa, the $f_{α'}$ increases with dose and approaches the saturation limit. On the other hand, the corresponding mean precipitate size $\overline{r_p}$ (not shown) is within 1.0-1.3 nm, and there is no evident trend of $\overline{r_{α'}}$ with dose. Therefore, for this specific condition, it is still in the nucleation regime. For other x_{Cr} or T_{irr}, it may enter growth regime at a lower dose. For instance, larger α′ precipitates with radius $\overline{r_{α'}}$ = 2-5 nm were

observed in Fe-Cr with x_{Cr} ~12% irradiated at 400°C to a dose of ~7 dpa [9][31]. However, a systematic investigation over a range of dose is currently not available because the irradiation data for those x_{Cr} and T_{irr} is limited.

5.2. Effects of Cr Concentration on the Irradiation-Enhanced α′ Precipitation

The α′ precipitation in Fe-Cr alloys is significantly dependent on x_{Cr}. Under equivalent irradiation condition, Fe-Cr alloys with higher x_{Cr} have larger $\overline{r_{\alpha'}}$, higher precipitate density $N_{\alpha'}$, higher α′ volume fraction $f_{\alpha'}$, and lower threshold dose for observable precipitation.

As shown in **Table 2**, $\overline{r_{\alpha'}}$ increases slightly with x_{Cr} at both 300°C and 450°C. This is consistent with the Monte Carlo modeling on thermally-aged bcc Fe-Cr [32][33]. Since the Cr diffusivity does not increase with x_{Cr}, the growth rate of precipitates is not the cause. Instead, the onset dose of nucleation accounts for this phenomenon. The precipitates in specimens with higher x_{Cr} nucleate α′ precipitates earlier and they have more time to grow. This is supported by the frequency analyses in this study, and by modeling [33]. Nevertheless, the $\overline{r_{\alpha'}}$ is relatively insensitive to x_{Cr}, consistent with other experiments and modeling [16][29] [30][32][33].

On the other hand, $N_{\alpha'}$ increases significantly with x_{cr}. This can be explained using the Gibb's homogeneous nucleation theory, expressed in Eq-5 [34].

$$\dot{N}_{\alpha'} \propto x_{Cr}\left[e^{\left(-\frac{\Delta G^*}{RT}\right)}\right] \qquad (Eq-5)$$

$N_{\alpha'}$ is the nucleation rate, ΔG^* is the activation energy for α-α' phase transformation, R is gas constant, and T is absolute temperature. ΔG^* decreases with x_{cr} because of the increasing driving force of phase transformation with x_{cr}. Since both x_{cr} and the exponential terms increase with x_{cr}, $\dot{N}_{\alpha'}$ increases with x_{cr}. The observation of this study that $N_{\alpha'}$, and not $\overline{r_{\alpha'}}$, varies strongly with x_{Cr} is in accordance with the modeling result in [33].

To study the x_{cr} effects on $f_{\alpha'}$, a compilation of experimental data is shown in Figure 10 for Fe-Cr ferritic alloys irradiated at about 300°C to a dose around 1 dpa. The dashed line is the α′ volume fraction predicted by the phase diagram in Ref. [28] using lever rule at 300°C. No α′ precipitation was observed below the threshold x_{Cr} of 8.1%, which is consistent with the prediction from the phase diagram. Beyond the threshold, $f_{\alpha'}$ increases with x_{Cr}. As discussed above, this is primarily due to the higher nucleation rate $\dot{N}_{\alpha'}$ in the specimens with higher x_{Cr}.

It needs to be mentioned that the comparisons in Figure 9 and Figure 10 involve uncertainties. The reported volume fractions were based on varied techniques where each technique has its own limitations and uncertainties. For instance, SANS does not detect cluster size smaller than 0.5 nm, resulting in a slight underestimation of volume fraction [35]. For APT, the trajectory aberration and local magnification effects can slightly change the obtained size of α′ precipitates [20]. In addition, the use of isosurface also introduces uncertainties because the apparent precipitate size and volume fraction depend on the Cr concentration chosen to define the isosurface, while the interface of α′ precipitates is not well defined.

5.3. Irradiation Temperature Effects on the Irradiation-Enhanced α′ Precipitation

As shown in Figure 1 and in Table 2, $\overline{r_{\alpha'}}$, $N_{\alpha'}$ and $f_{\alpha'}$ of α′ precipitate in Fe-Cr specimens decrease with T_{irr}. This is in agreement with the prediction from the phase diagram in [28] that $f_{\alpha'}$ decreases with increasing T_{irr}. The observation of lower $N_{\alpha'}$ with higher T_{irr} might be attributed to a decreasing nucleation rate $\dot{N}_{\alpha'}$ with increasing T_{irr}. In terms of Gibb's homogeneous nucleation theory in Eq-5 [34], T_{irr} has effects on both the ΔG^* and the RT terms. When T_{irr} increases, the RT terms result in an increase in $\dot{N}_{\alpha'}$. On the other hand, increasing T_{irr} results in a reduction in the driving force for precipitation, leading to an increase in ΔG^*, and therefore, and a decrease in $\dot{N}_{\alpha'}$. In this case, the effect of increasing T_{irr} on the ΔG^* term is inferred to be more significant than on RT term.

The size $\overline{r_{\alpha'}}$ decreases with increasing T_{irr}. Compared to x_{Cr}, the effect of T_{irr} on $\overline{r_{\alpha'}}$ is more significant. The Cr diffusivity is not applicable to interpret this temperature dependence because increasing T_{irr} should enhance Cr diffusivity and the precipitate growth rate, provided diffusion-controlled mechanism. Therefore, there must be other mechanism controlling the growth of α' precipitate. Perhaps, the smaller $\overline{r_{\alpha'}}$ with T_{irr} is due to the smaller $\dot{N_p}$ that come with a delayed onset for precipitation growth. These questions remain unclear at this point.

5.4. The Core Cr Concentration Dependence on the Size of α′ Precipitates

As Figure 4 shows, the majority of precipitates in this study had a core Cr concentration considerably below the equilibrium concentration predicted by the phase diagram (>90%). Several hypotheses have been proposed to explain this APT observation, such as the non-classical nucleation, the modified phase diagram and APT artifacts. The non-classical nucleation explanation is not favored due to the low nominal Cr contents in this study [14][16]. The irradiation-induced point defects (super-saturated) have been suggested to change the phase diagram, resulting in a higher Fe solubility in Cr [15][16]. However, this can not explain the observed correlation between the core Cr concentration and precipitate sizes.

The blurring of the APT data at the interface could cause a deficit of precipitate component (Cr for this study) in very small clusters [21]. As the size of the precipitate increased, the blurring effects at the interface became less significant and therefore the core Cr concentration would approach the equilibrium value. This hypothesis is more in agreement with the concentration-size correlation. Finally, another plausible explanation from the work of Svetukhin et al. showed that the precipitate composition is determined by the interface surface energy in the Fe-Cr binary system, resulting in increasing Cr content of α' precipitates with increasing precipitate size [36]. To justify these hypotheses, further studies combining experiments, atom probe simulation and thermodynamic calculations are required.

Conclusion

Ferritic Fe-Cr model alloys have been irradiated with neutrons at 300 and 450°C to the doses of 0.01, 0.1 and 1 dpa. Atom probe tomography has been performed to investigate the α-α' decompositions in those specimens. The α' precipitates of size of 1-2 nm appeared in all of the 1 dpa specimens. The relative volume fraction between individual specimens was consistent with the prediction from the phase diagram. The density of α' precipitates increases significantly with increasing Cr content and decreasing irradiation temperature. The size of α', however, is relatively insensitive to the Cr content and the irradiation temperature.

In Fe-10Cr poly-crystals of doses equal and less than 0.1 dpa, no Cr segregation could be detected with the analysis techniques employed in this study. On the other hand, some increases in Cr segregation were observed in single-crystalline specimens (with higher Cr content) of equivalent dose by the use of frequency distribution analysis.

The Cr concentration profiles of the α' precipitates in the 1 dpa specimens were examined using proxigram analysis. The profiles were similar for all of the conditions; i.e. Cr concentration increased toward the precipitate core without forming a plateau. In addition, it has been shown that core Cr concentration increased with precipitate size.

This work provides experimental information on the microstructure evolution of Fe-Cr model alloys under neutron irradiation in atomic scale as a function of Cr concentrations and irradiation temperatures. The results are useful for understanding the mechanical property degradation of F/M steels, and could serve as the benchmark for atomistic simulations in this class of materials.

Acknowledgement

References

[1] R.L. Klueh, K. Ehrlich, F. Abe, J. Nucl. Mater. 116 (1992) p. 191

[2] R.L. Klueh, D.R. Harries, ASTM Monograph 3, American Society for Testing and Materials, West Conshohocken, PA, 2001

[3] T. Lechtenberg, "Irradiation effects in ferritic steels," J. Nucl. Mater. 133-134 (1985), p. 149

[4] A. Koyama, A. Hishinuma, D.S. Gelles, R.L. Klueh, W. Dietz and K. Ehrlich, "Low-activation ferritic and martensitic steels for fusion application," J. Nucl. Mater. 233-237A (1996), p. 138

[5] M. Matijasevic, A. Almazouzi, "Effect of Cr on the mechanical properties and microstructure of Fe–Cr model alloys after n-irradiation," J. Nucl. Mater. 377 (2008) p.147

[6] Z. Yao, M. Hernandez-Mayoral, M. Jenkins and M.A. Kirk, "Heavy-ion irradiations of Fe and Fe-Cr model alloys part I: Damage evolution in thin-foils at lower doses," Philosophical Magazine 88 (2008), p. 2851

[7] M. Hernandez-Mayoral, Z. Yao, M. Jenkins and M.A. Kirk, "Heavy-ion irradiations of Fe and Fe-Cr model alloys part I: Damage evolution in thin-foils at higher doses," Philosophical Magazine 88 (2008), p. 2881

[8] M. Jenkins, Z. Yao, M. Hernandez-Mayoral, and M.A. Kirk, "Dynamic observation of heavy-ion damage in Fe and Fe-Cr alloys," *Journal of Nuclear Materials* 389 (2009), p.197

[9] S.I. Porollo, A.M. Dvoriashin, A.N. Vorobyev, Yu.V. Konobeev, "The microstructure and tensile properties of Fe-Cr alloys after neutron irradiation at 400°C to 5.5-7.1 dpa." Journal of Nuclear Materials 256 (1998), p.247

[10] Y.V. Konobeev, A.M. Dvoriashin, S.I. Porollo and F.A. Garner, "Swelling and microstructure of pure Fe and Fe–Cr alloys after neutron irradiation to ~26 dpa at 400 °C," Journal of Nuclear Materials 355 (2006), p.124

[11] F. Danoix and P. Auger, "Atom probe studies of the Fe-Cr system and stainless steels aged at intermediate temperature: a review," Materials Characterization 44 (2000), p. 177

[12] M.K. Miller, J.M. Hyde, M.G. Hetherington, A. Cerezo, G.D.W. Smith and C.M. Elliott, "Spinodal decomposition in Fe-Cr alloys: Experimental study at the atomic level and comparison with computer models—I. Introduction and methodology," Acta Metallurgica et Materialia 43 (1995), p. 3385

[13] P. Auger, F. Danoix, A. Menand, S. Bonnet, J. Bourgoin, and M. Guttmann, "Atom probe and transmission electron microscopy study of aging of cast duplex stainless steels," Material Science and Technology 6 (1990), p. 301

[14] S. Novy, P. Pareige, C. Pareige, "Atomic scale analysis and phase separation understanding in a thermally aged Fe–20 at.%Cr alloy," Journal of Nuclear Materials 384 (2009), p. 96

[15] M.K. Miller, R. Stoller and K. Russell, "Effect of neutron-irradiation on the spinodal decomposition of fe-32%cr model alloys," J. Nucl. Mater. 230 (1996), p.219

[16] V. Kuksenko, C. Pareige, C. Genevois, F. Cuvilly, M. Roussel, P. Pareige, "Effect of neutron-irradiation on the microstructure of a Fe–12at.%Cr alloy," Journal of Nuclear Materials 415 (2011), p61

[17] M. Bachhav, G.R. Odette, E.A. Marquis, "α′ precipitation in neutron-irradiated Fe-Cr alloys," Scripta Materialia 74 (2014), p. 48

[18] M.K. Miller and R.G. Forbes, "Atom Probe Tomography," Materials Characterization 60 (2009), p.461

[19] M.P Moody et al., "Quantitative Binomial Distribution Analyses of Nanoscale Like-Solute Atom Clustering and Segregation in Atom Probe Tomography Data," Microscopy Research and Technique 71 (2008), p.542

[20] M.K. Miller, "Atom Probe Tomography: Analysis at the atomic level," Kluwer Academic/Plenum Publisher. (2000) New York

[21] Hellman et al., "Analysis of Three-dimensional Atom-probe Data by the Proximity Histogram," Microscopy and Microanalysis 6 (2000), p. 437

[22] V. Kuksenko, C. Paeige, C. Genevois, F. Cuvilly, M. Roussel, P. Paeige, "Effect of neutron-irradiation on the microstructure of a Fe-12at.%Cr alloy," Journal of Nuclear Materials 415 (2011), p.61

[23] P. Olsson, I.A. Abrikosov, L. Vitos, J. Wallenius, "Ab initio formation of energies of Fe-Cr alloys," Journal of Nuclear Materials 321 (2003), p. 84

[24] E.A. Marquis, J.M. Hyde, "Applications of atom-probe tomography to the characterisation of solute behaviours." Materials Science and Engineering R 69 (2010), p. 37

[25] T. Hamaoka, A. Nomoto, K. Nishida, K. Dohi, N. Soneda. "Effects of aging temperature on G-phase precipitation and ferrite-phase decomposition in duplex stainless steel." Philosophical Magazine 92 (2012), p. 4354

[26] K. Fujii and K. Fukuya. "Effects of radiation on spinodal decomposition of ferrite in duplex stainless steel." Journal of Nuclear Materials 440 (2013), p.612

[27] G. Bonny, D. Terentyev, L. Malerba, "On the α–α′ miscibility gap of Fe–Cr alloys," Scripta materialia 59 (2008), p. 1193

[28] Malerba et al. "Multiscale modeling of radiation damage and phse transformations: The challenge of FeCr alloys," Journal of Nuclear Materials 382 (2008), p. 112

[29] V. Kuksenko, C. pareige, P. pareige, "Cr precipitation in neutron irradiated industrial purity Fe-Cr model alloys", Journal of Nuclear Materials 432 (2013), p.160

[30] M.H. mathon, Y. de Carlan, G. Geoffroy, X. Averty, A. Alamo, C.H. de Novion, "A SANS investigation of the irradiation-enhanced α–α′ phases separation in 7-12 Cr martensitic steels. " Journal of Nuclear Materials 312 (2003), p. 236

[31] Z. Jizo, V. Shankar, G.S. Was, "Phase stability in proton and heavy ion irradiated ferritic-martensitic alloys." Journal of Nuclear Materials 419 (2011), p. 52

[32] M.Yu. Lavrentiev, R. Drautz, D. Nguyen-Manh, T.P.C. Klaver, S.L. Dudarev, "Monte Carlo study of thermodynamic properties and clustering in the bcc Fe-Cr system. " Physical Review B 75 (2007), p.014208

[33] G. Bonny, D. Terentyev, L. Malerba, D. Van Neck, "Early stages of α-α' phase separation in Fe-Cr alloys: An atomistic study." Physical Review B 79 (2009), p. 104207

[34] J.W. Gibbs, Trans. Conn. Acad. Arts Sci. 3, 102 (1878)

[35] E. Meslin, M. Lambrecht, M. Hernández-Mayoral, F. Bergner, L. Malerba, P. Pareige, B. Radiguet, A. Barbu, D. Gómez-Briceño, A. Ulbricht, A. Almazouzi, "Characterization of neutron-irradiated ferritic model alloys and a RPV steel from combined APT, SANS, TEM and PAS analyses." Journal of Nuclear Materials 406.1 (2010), p. 73.

[36] V. Svetukhin, P. L′vov, E. Gaganidze, M. Tikhonchev, C. Dethloff, "Kinetics and thermodynamics of Cr nanocluster formation in Fe–Cr system," Journal of Nuclear Materials 415 (2011), p. 205

[37] C. Heintze, F. Bergner, A. Ulbricht, H. Eckerlebe, "The microstructure of neutron-irradiated Fe-Cr alloys: A small-angle neutron scattering study." Journal of Nuclear Materials 409 (2011), p. 106

[38] R. Coppola, R. Lindau, R.P. May, A. Möslang, M. Valli, "Investigation of microstructural evolution under neutron irradiation in Eurofer97 steel by means of small-angle neutron scattering. " Journal of Nuclear Materials 386 (2009), p.195
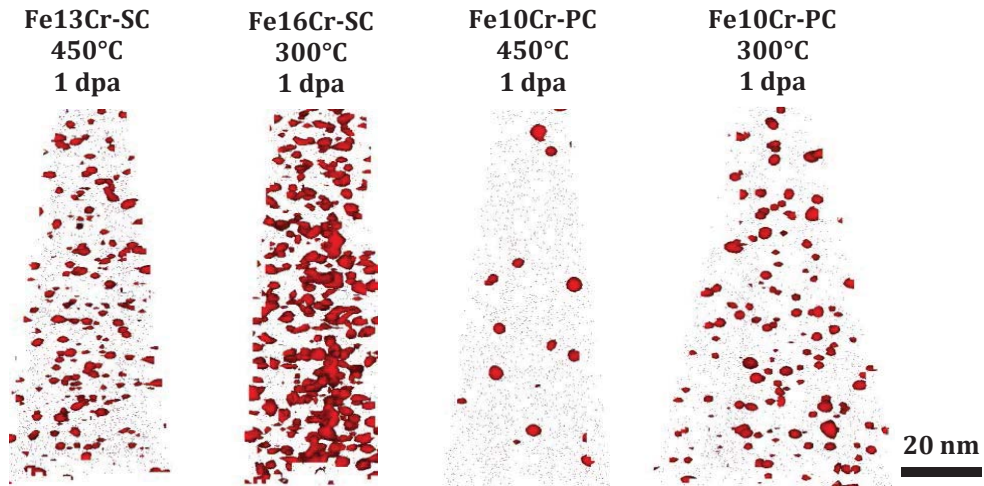
Figure 1. The reconstructed APT images of the 20%Cr isosurfaces of Fe-Cr model alloys irradiated by neutrons to a dose of 1 dpa at 300°C and 450°C.
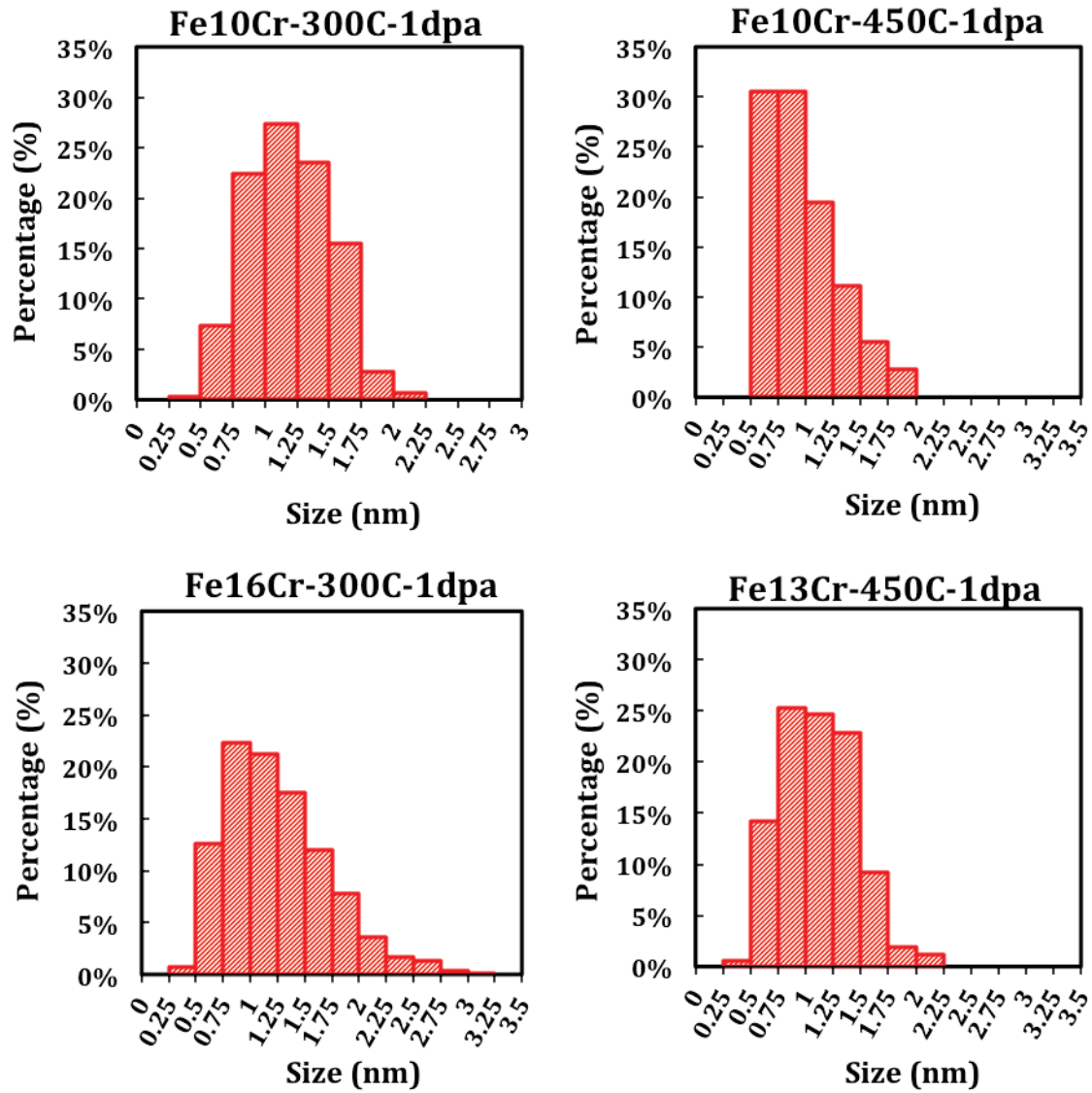
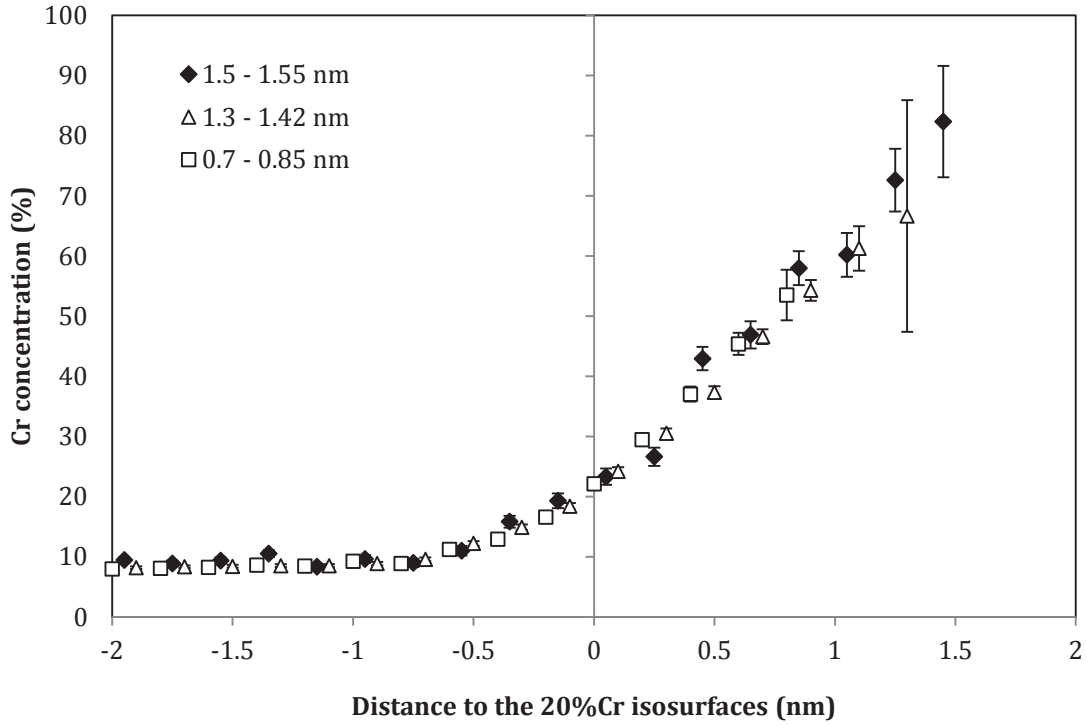Figure 2. The size distribution of α′ precipitates in Fe-Cr model alloys irradiated to 1 dpa.

Figure 3. The proxigrams to the 20%Cr isosurfaces of α′ precipitates in Fe10Cr-PC specimens irradiated at 300°C to 1 dpa. Three size groups are plotted: $\overline{r_{\alpha'}}$ = 1.5 – 1.55 nm, 1.3 – 1.42 nm and 0.7 – 0.85 nm.
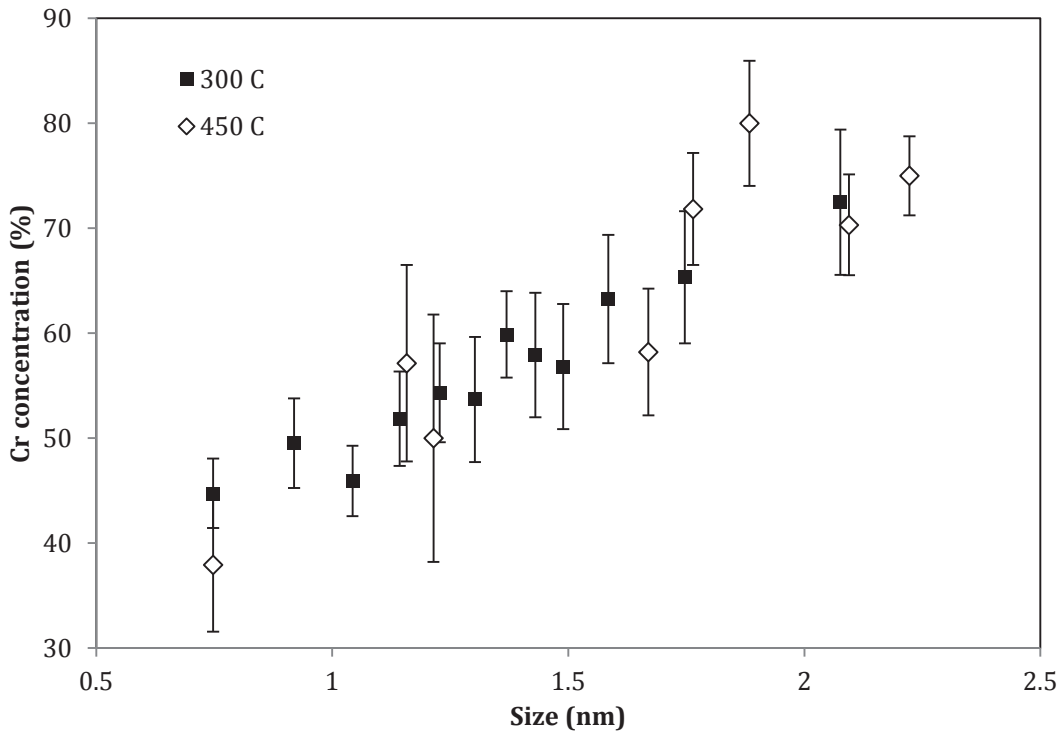

Figure 4. The core Cr concentration at the center of α′ precipitates as a function of precipitate size in radius in 1 dpa Fe10Cr-PC specimens irradiated at 300 and 450°C
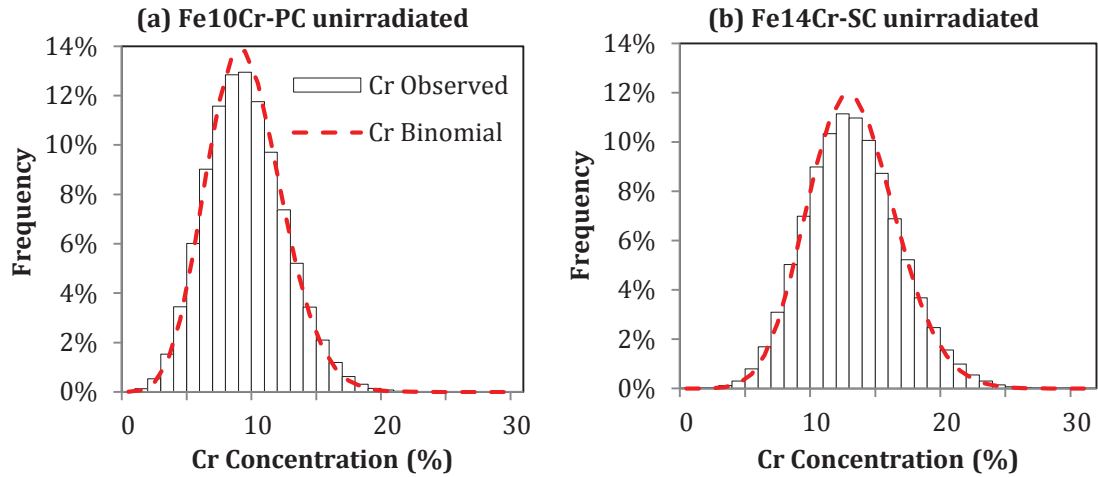
Figure 5. Frequency distribution of un-irradiated (a) Fe10Cr-PC specimen and (b) Fe14Cr-SC specimens.
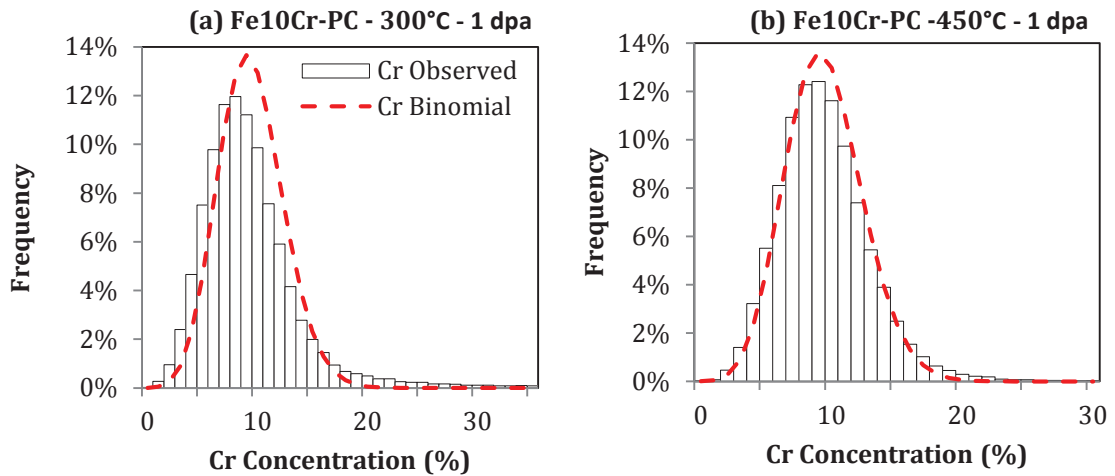

Figure 6. Frequency distribution for 1 dpa poly-crystalline Fe10Cr-PC specimens irradiated (a) at 300°C and (b) at 450°C.
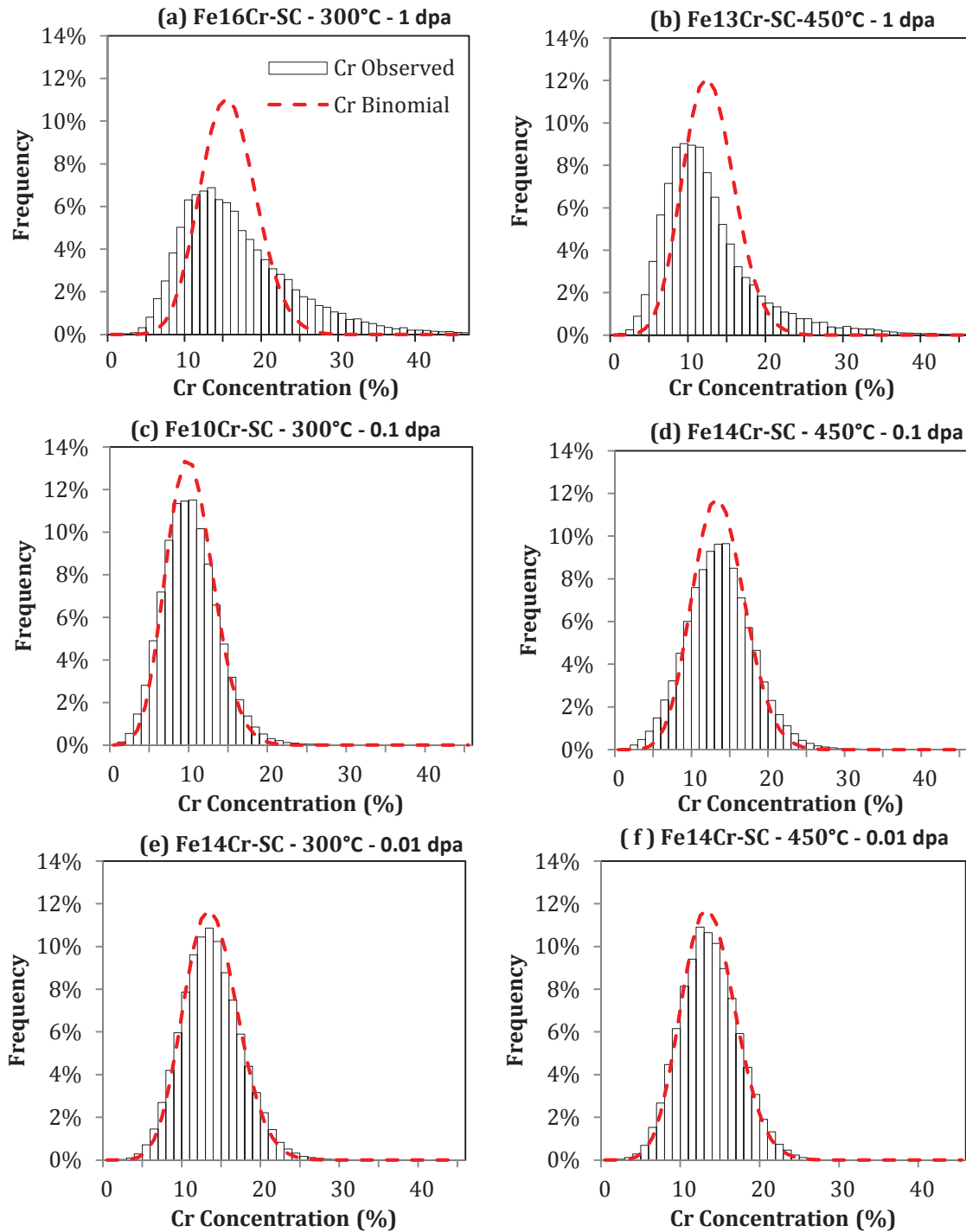
Figure 7. Frequency distribution analysis for single-crystalline specimens irradiated at 300°C to a dose of (a) 1 dpa and (c) 0.1 dpa (e) 0.01 dpa, and at 450°C to the doses of (b) 1 dpa and (d) 0.1dpa (f) 0.01 dpa. The bin size n_b is 100.
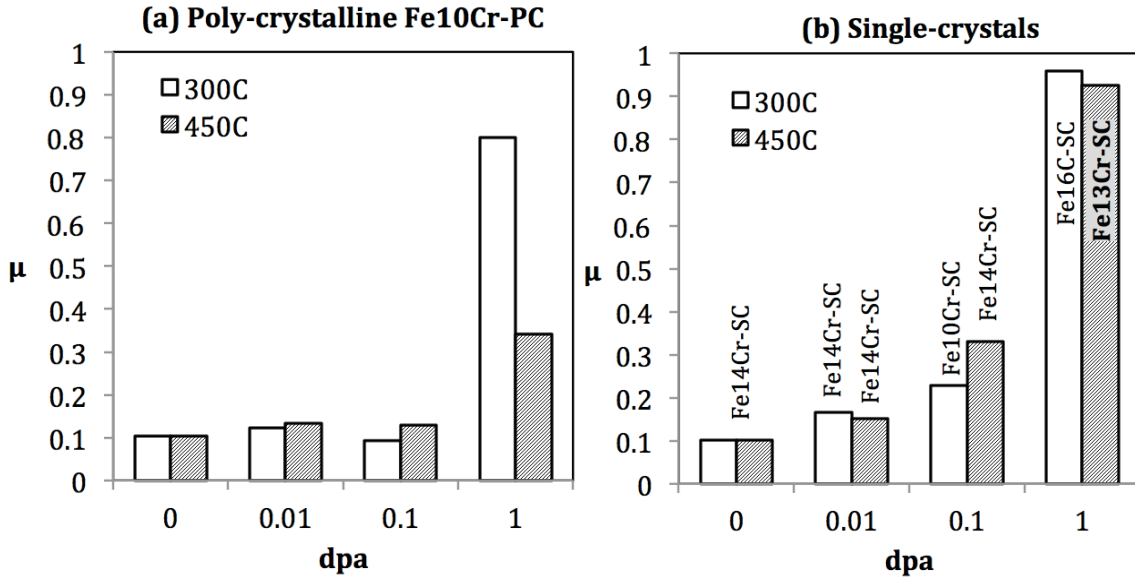
Figure 8. The μ-index of un-irradiated and irradiated (a) poly-crystalline Fe10Cr and (b) single-crystalline specimens, based on the frequency distribution analysis.
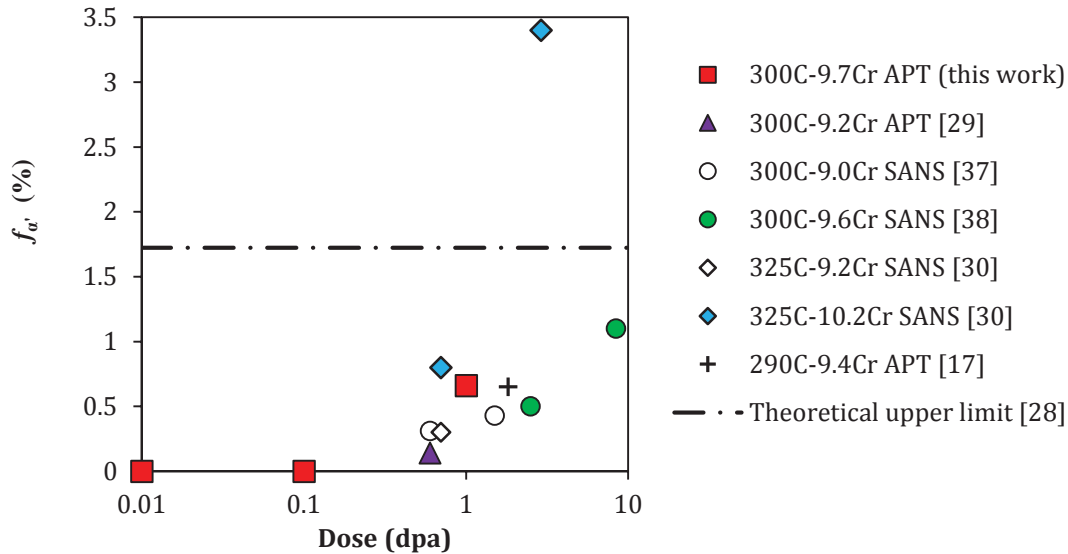

Figure 9. α' volume fraction deduced from APT and SANS for Fe-Cr model alloys and commercial F/M steels irradiated to doses of 0.6-8.4 dpa with Cr concentration x_C=9-10% and irradiation temperature T_{irr} = 300-325°C. The dashed line is the saturation limit calculated for Fe-Cr alloys with x_{Cr}=9.65% at 300°C.
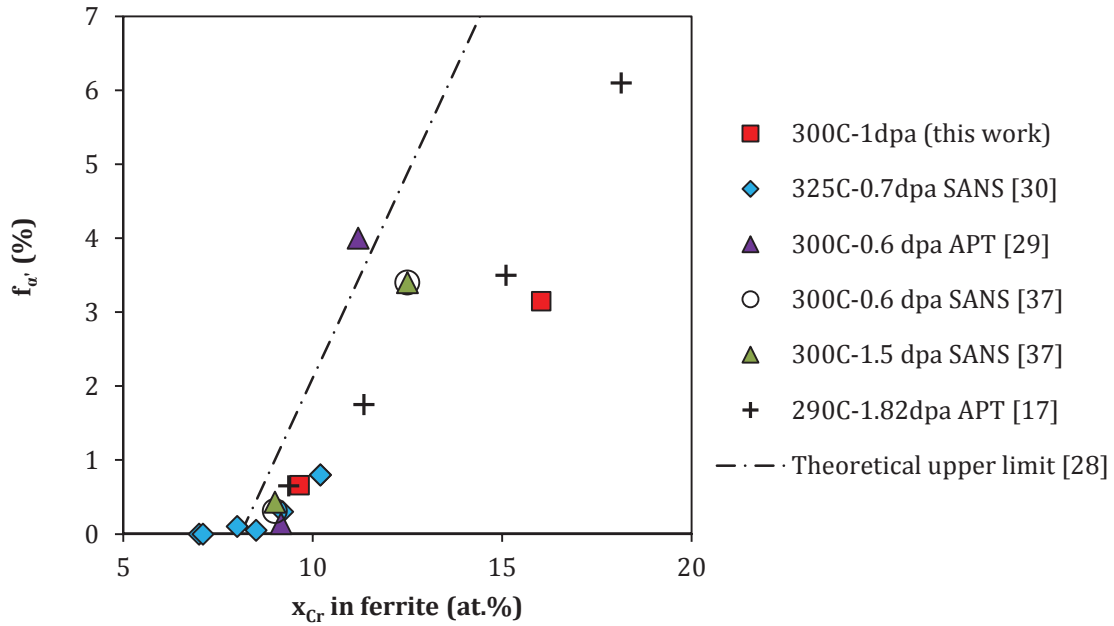
Figure 10. α' volume fraction $f_{\alpha'}$ deduced from APT and SANS on Fe-Cr model alloys and commercial F/M steels with Cr concentration x_{Cr} of 7-16 at.% with a irradiation temperature and a dose close to 300°C and 1 dpa, respectively. The dashed line is the saturation limit calculated for Fe-Cr alloys at 300°C.

Table 1. Nominal irradiation conditions and measured Cr concentrations of Fe-Cr single crystals

	Specimen Label	Irradiation Conditions	x_{Cr} (at.%)
Poly-crystals	Fe10Cr-PC	300, 450°C No irradiation, 0.01, 0.1, 1 dpa	9.65
Single-Crystals	Fe13Cr-SC	1 dpa – 450°C	12.93 ± 0.02
	Fe16Cr-SC	1 dpa – 300°C	16.03 ± 0.03
	Fe14Cr-SC	0.1 dpa – 450°C	14.18 ± 0.02
	Fe10Cr-SC	0.1 dpa – 300°C	10.02 ± 0.02
	Fe14Cr-SC	0.01 dpa – 450°C	14.14 ± 0.02
	Fe14Cr-SC	0.01 dpa – 300°C	13.95 ± 0.01
	Fe14Cr-SC	No irradiation	13.67 ± 0.01

Table 2. The density, mean size and volume fraction of α' precipitates in Fe-Cr model alloys irradiated to 1 dpa. The error represents the standard deviation from the mean value.

Specimen	Irradiation condition	$N_{\alpha'}$ (x10²³ m⁻³)	$\overline{r_{\alpha'}}$ (nm)	$f_{\alpha'}$ (%)
Fe10Cr-PC	300 °C-1 dpa	7.7	1.18 ± 0.32	0.66
Fe10Cr-PC	450 °C-1 dpa	1.1	1.00 ± 0.36	0.072
Fe16Cr-SC	300 °C-1 dpa	27	1.25 ± 0.47	3.2
Fe13Cr-SC	450 °C-1 dpa	13	1.08 ± 0.32	0.85